08,03

Influence of the external field and temperature on the temporal evolution of the leakage current in the $BiFeO_3/TiO_2(Nt)Ti$ film structure

© G.M. Gadzhiev, Sh.M. Ramazanov ¶, N.S. Abakarova, T.N. Efendieva

Amirkhanov Institute of Physics, Dagestan Federal Research Center, Russian Academy of Sciences, Makhachkala, Dagestan Republic, Russia

¶ E-mail: ramazanv@mail.ru

Received October 13, 2023
Revised January 15, 2024
Accepted January 18, 2024

The behavior of leakage currents of the $BiFeO_3/TiO_2(Nt)$ film structure has been studiedTi (BFOT) obtained by atomic layer deposition of bismuth ferrite on a substrate of pre-prepared titanium dioxide nanotubes, depending on the exposure time and the magnitude of the electric voltage in the temperature range of $28-250^{\circ}C$. Electrically inhomogeneous states with a volume charge arise in the BFOT structure, which leads to hysteresis of the VAC. Hysteresis and heterogeneity depend on the relaxation time. The time dependence of the leakage currents revealed features in the form of a tendency to form a maximum in the temperature range $\sim 28-200^{\circ}C$. At a temperature of $T = 250^{\circ}C$, the maximum is stabilized on a time dependence and grows monotonously with an increase in the applied voltage. For this structure, the characteristic time $t = 0.5$ s for dependencies $I(t)$ is determined due to the capture and release of carriers from defective levels.

Keywords: $BiFeO_3$, leakage current, nanotubes, thin films.

DOI: 10.61011/PSS.2024.02.57921.227

1. Introduction

Modern micro- and nanoelectronics places increasingly stringent requirements to information storage devices: it is necessary to manufacture new types of storage devices that combine the high-speed characteristics of RAM with the non-volatility of Flash memory. Such universal memory shall have an unlimited number of write/read cycles, low power consumption and cost, provide high information density and the potential for further scaling [1]. Ferroelectric (FeRAM) and resistive (ReRAM) memories are considered as promising candidates for creating the new generation of memory devices that meet the above requirements. From this point of view, recently, multiferroic $BiFeO_3$ (BFO), which combines the magnetoelectric effect and the resistive switching effect (RS) attracted great interest of researchers [2]. BFO thin films, both epitaxial and polycrystalline, due to their excellent properties [3–8]: residual polarization P_r, inverse piezoelectric effect, comparable to those of tetragonal PZT system enriched with Ti and high Curie temperature $T_C = 820-850^{\circ}C$ are promising materials for application in various aspects of micro- and nanoelectronics.

Leakage currents are considered undesirable in thin-film dielectrics (ferroelectrics) when used in memory elements. At the same time, when using film structures as artificial synapses in neuromorphic applications, the dynamics of changes in leakage currents plays an important role in the memorization process [9]. In this sense, the study of the mechanisms of leakage currents in nano- and microelectronics elements is an urgent task. Among the papers devoted to the study of the evolution of leakage currents in BFO thin films at a constant voltage, attention is mainly paid to studying the behavior of the leakage current either in a very narrow time interval (from ns to ms) or in a too wide one (up to several hours) [2,9–13]. There are practically no papers that analyze the current dependence on time in the range from several ms to sec. Such studies may be of interest in the areas of field-effect transistors creation on a ferroelectric basis and in applications using artificial synapses close to natural analogues.

In this paper we report the features of leakage currents in film structure based on BFOT depending on the magnitude of the electric field and the duration of its exposure $(0-1.0\,s)$ at different sample temperatures.

2. Specimens and experimental methods

BFO films were grown by atomic layer deposition (ALD) on ALDCERAM ML-200 unit. A titanium plate was used as a substrate, on which $TiO_2(Nt)$ film in the form of vertical nanotubes was previously obtained by electrochemical method. The ALD method makes it possible to obtain films with 100% conformity, which is relevant for the chosen system. The thickness of $TiO_2(Nt)$ layer was $\sim 2.5\,\mu m$. $Bi(mmp)_3$(tris(1-methoxy-2-methyl-2-propoxybismuth) and ferrocene $Fe(cp)_2$ were used as sources of precursors. In ALD method the precursors were delivered to the chamber using a carrier gas N_2 with a purity of 99.999%. The temperature range of $Bi(mmp)_3$ evaporation was $135-145^{\circ}C$, the evaporation temperature of ferrocene was $90^{\circ}C$. ALD BiO_xconsisted of Bi $(mmp)_3$

precursor pulse with width of 1.2 s, then purging with N_2 admission of pulse of O_3 — 5 s, in the interval between cycles nitrogen purging was carried out for 15 s. Cycles of ALD FeO_x were then applied. The pulse width of $Fe(C_5H_5)_2$ precursor — 2 s. The number of admission subcycles of each precursor was 90. Throughout the entire experiment, the inlet and outlet gas pipelines were maintained at a temperature of 150°C. The substrate was located at a distance of 4–5 cm from the inlet. The rector was uniformly heated to 250°C. Afterwards, the resulting samples were heat treated in air at temperature of 660°C for 60 min. To carry out electrical measurements, the contacts were deposited on the surface using magnetron sputtering, and a titanium substrate served as the bottom electrode. The experimental part of the fabrication of this structure is described in more detail in paper [14].

Electrical measurements were performed on Keithley 2400 source-meter. The voltage sweep when measuring the current-voltage curve (CVC) was carried out in the form of a bidirectional triangular signal (0 V → 15 V → 0 V → −15 V → 0 V). At each sweep point the measurement was carried out according to the following scheme: voltage generation–delay (waiting)–current measurement. The delay varied from 0.01 s to 2 s. The instrument normal option of speed measurement was selected. The sample temperature was set by a resistive heater and monitored by K type. thermocouple.

3. Results and discussion

In the BFOT structure a change in resistance occurs when voltage is applied with the formation of phase boundaries and the redistribution of oxygen vacancies. In the presence in the structure of Fe and Ti ions with oxidation states different from the homogeneous crystal structure, the oxygen vacancies necessary to maintain the electrical neutrality of the system are induced. The formation of oxygen vacancies reduces intrinsic defects, which are well-known capture centers for carriers recombination. This effect promotes electron-hole separation. The appearance of Ti^{3+} is caused by the fact that Fe atoms partially replace titanium atoms in TiO_6 octahedra. Similarly to $Fe^{3+} \rightarrow Fe^{2+}$ transition, during $Ti^{4+} \rightarrow Ti^{3+}$ transition the replacement leads to increase in the ferroelectric residual polarization. And there is also increase in the hybridization of Bi 6*s* electrons with 2*p* oxygen place, which contributes to the generation and enhancement of hole mobility and a shift in the edge of the valence band. In BFOT structure, when a bias is applied, the inhomogeneous regions with different conductivities are formed [15].

Figure 1 shows CVC of the BFOT film structure measured at different voltage sweep rates (delay times). The given C–VCs were obtained without preliminary electroforming of the sample, i. e. in high resistance state.

From Figure 1 it is clear that CVCs of the sample are characterized by the presence of a hysteresis loop passing

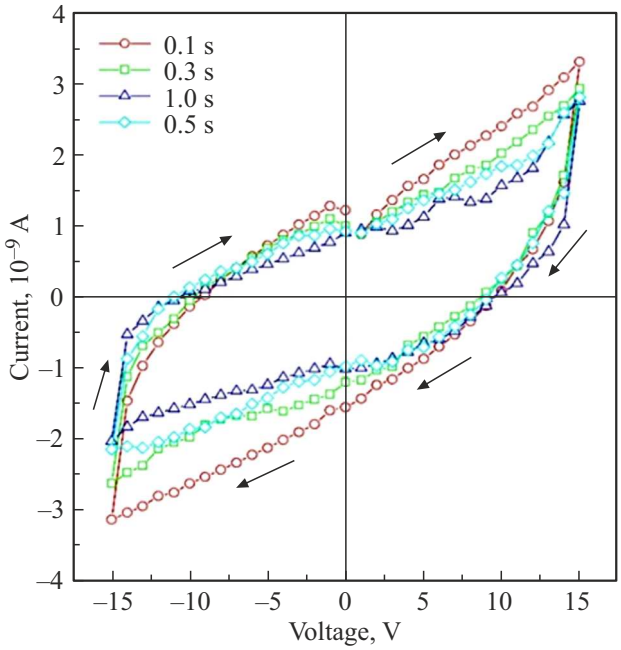

Figure 1. CVC of the sample, measured with different delay times. The arrows indicate the direction of circulation the loop during voltage sweep.

through all four quadrants of C–V coordinates. With increase in the voltage sweep rate, CVC loop slightly expands in the first and third quadrants, which is due to increase in the bias current, defined as the time derivative of the electrical displacement D [16]. An insignificant maximum in the initial section of the forward path of the current-voltage characteristic for a delay time of 1.0 s is associated with the switching of polarization domains in the ferroelectric along the external field [16].

As a rule the cigar-shaped loops of CVC (Figure 1) are explained by the appearance of the internal field due to space-charge polarization in the inhomogeneous structure of the dielectric [17], which in our case is ensured by the two-layer nature of the sample. The internal electric field is directed towards the external one and at the point of intersection of the backward path of the curve $I(V)$ with the abscissa axis compensates it completely; with further decrease in voltage the internal field prevails over the external one — the current changes its direction to the opposite (Figure 1, 1st quadrant). To test this assumption, we measured CVC with the voltage reset to zero before each next step of the voltage sweep (Figure 2), while the absence of voltage and the action time (delay time) of the next voltage step were equal.

With such a sweep scheme, as can be seen from Figure 2, CVC loops merge into a line. On the ordinate of the middle CVC (Figure 2), the dots indicate the current values after the voltage reset to zero from the corresponding values (dashed lines). Negative current values after zeroing of positive voltage values and positive currents after resetting

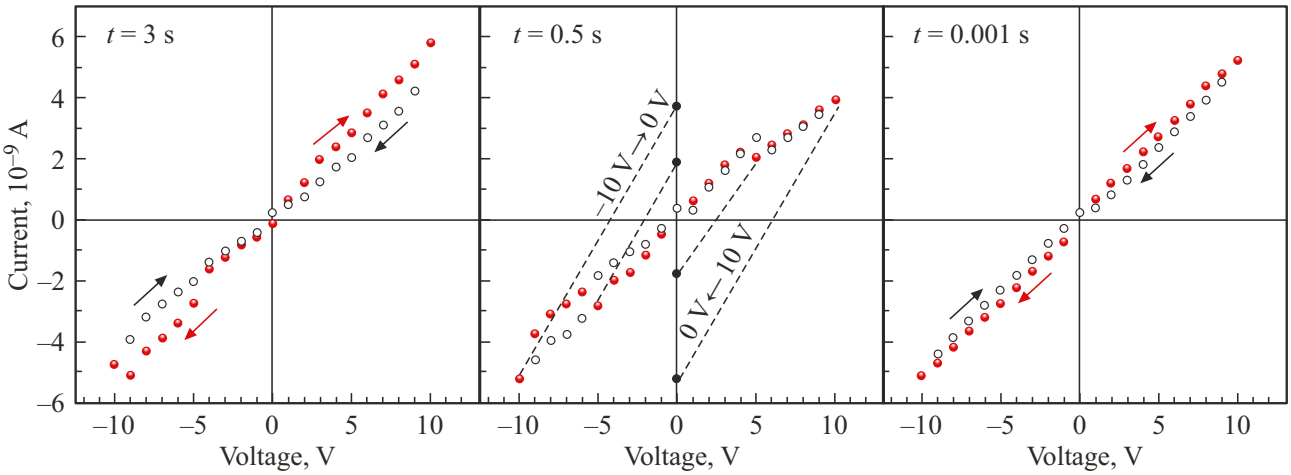

Figure 2. CVC of the sample, measured with the voltage reset to zero before each subsequent sweep step. The measurement delay time is indicated in the upper left corner. Red circles correspond to the forward motion $I(V)$ of dependence in the region of positive and negative voltages.

negative voltages indicate the presence of internal electric field in the sample, directed towards the external one. Figure 3 shows the behavior of CVC loops of the sample at different temperatures, measured with time delay $t = 0.1$ s.

The Figure, shows that as the temperature increases, C−VC loop narrows along the ordinate axis, at the same time, the current values along the loop contour increase and at $T = 250°C$ the loop degenerates into the line, and the current value at the end of the forward path $I(V)$ by ~ 50 times is greater than the corresponding value for $T = 28°C$. The increase in conductivity with temperature increasing is due to increase in carrier concentration. In turn, the increase in conductivity complicates polarization processes in the dielectric (ferroelectric), since these are competing mechanisms; therefore, the internal field in the sample weakens as it heats up, which ultimately leads to the collapse of CVC loop.

The characteristic feature of the dependence $I(t)$ of the sample at $T = 28$, 100 and 200°C is the gradual decrease in current with time after connecting constant voltage with further plateau achievement. Visual continuation of the descending part of the curves $I(t)$ for 10, 15 V at $T = 28°C$ and all curves at $T = 100°C$ intersect the abscissa axis in the region of $\sim 0.4-0.5$ s. The time dependence of the current for 10 and 15 V at $T = 100°C$ and for 10 V at $T = 200°C$ indicates a weak manifestation of the maximum in the vicinity of time $t = 0.5$ s (Figure 4).

At temperature $T = 250°C$ the maximum in the time dependence stabilizes and begins to grow monotonically with applied voltage increasing. Thus, $t = 0.5$ s is a characteristic time for dependencies $I(t)$.

The behavior of the current over time after turning off the external voltage of the corresponding value is shown in Figure 5. The internal polarization field generates a negative current (the current values in Figure 5 are indicated in absolute value) after turning off the voltage, and at that for the dependences *1, 2* and *3* (Figure 5) current relaxation in the interval $t = 0-0.3$ s and a weak maximum at $t = 0.5$ s are observed. Curves *4* and *5* illustrate a slight increase in current after turning off the external voltage.

In the initial period of time a rapidly decreasing bias current I_{cm} flows in the circuit, stopping in time approximately equal to the time constant of the RC circuit „source−sample“. The slowly changing component of the current (Figure 4, $T = 28°C$), caused by the redistribution of free charges in the volume of the dielectric — absorption current I_{abs}. This current is associated with the absorption of charge carriers by the volume of the dielectric: some of the carriers meet capture traps–lattice defects on their way, they capture and retain carriers. In our case, such traps can be oxygen vacancies, which inevitably arise in the sample at one of the technological stages of the film structure manufacturing.

Possible mechanisms of conductivity in ferroelectric films (dielectrics) are Schottky and Poole-Fraenkel emissions, Fowler-Nordheim tunneling, current (both ohmic and space charge limited (SCLC) and conductivity between grain boundaries [18]. The Schottky emission current is thermoelectron emission, with the process facilitated by the application of an electric field, which is expressed by the formula [17]:

$$J_s AT^2 \exp\left[\frac{W_b}{kT} - \frac{1}{kT}\left(\frac{q^3 V}{4\pi\varepsilon\varepsilon_0 d}\right)^{1/2}\right], \qquad (1)$$

where A — Richardson's constant, W_b — the height of the potential barrier without taking into account its decreasing by electric image forces, ε — dielectric permittivity of film material in the optical region, ε_0 — dielectric constant, d — film thickness, V — external voltage, q — charge unit, k — Boltzmann constant, t — temperature.

During Poole-Frenkel emission the carriers trapped at defect levels in the dielectric volume are emitted from

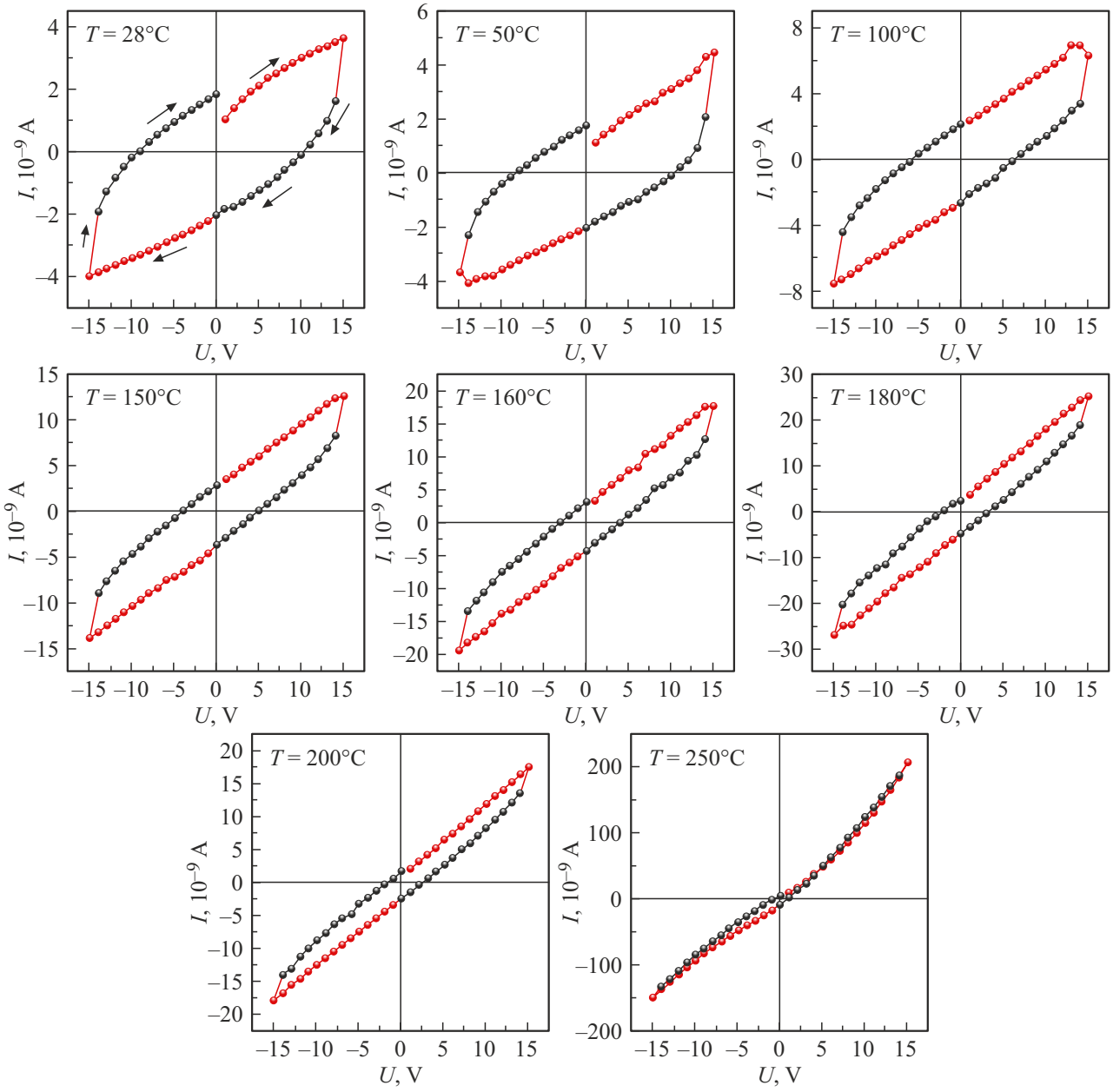

Figure 3. CVC of the film at different temperatures, delay time $t = 0.1$ s. Red dots — forward path, black dots — backward path.

the band gap into the conduction band upon application of field sufficient to change the defect potential. The current is determined by the distribution of defect levels in the film volume and depends on temperature and the applied field. The expression for the current due to Poole-Frenkel emission is similar to the expression for Schottky emission. However, in this case, the depth of the trap is determined by the depth of the level I_t in the band gap (counted down from the bottom of the conduction band, in the case of donor defects), and not by the height of the energy barrier W_b at the electrode interface–film, and the barrier decreasing turns out to be by 2 times greater, which is due to the immobility of the trap charge [18]. The energy W_b determined from the slope of the direct temperature dependence of the current (I), plotted in the coordinates $\mathrm{Ln}(J/AT^2) - 1/T$ at voltages 5, 10 and 15 V amounted to 0.41, 0.44 and 0.51 eV, respectively (Figure 6). The insert in Figure 6 shows a picture of a linear increase in energy W_b with external voltage increasing. The temperature dependence $J(T)$ was plotted using data from the forward path (region of positive voltages) of CVC at different temperatures with measurement delay time $t = 0.5$ s.

Relaxation time of level filling τ determines the time the current carrier remains at the level of E_t trap and the time of its emptying after turning off/on the activation process, in

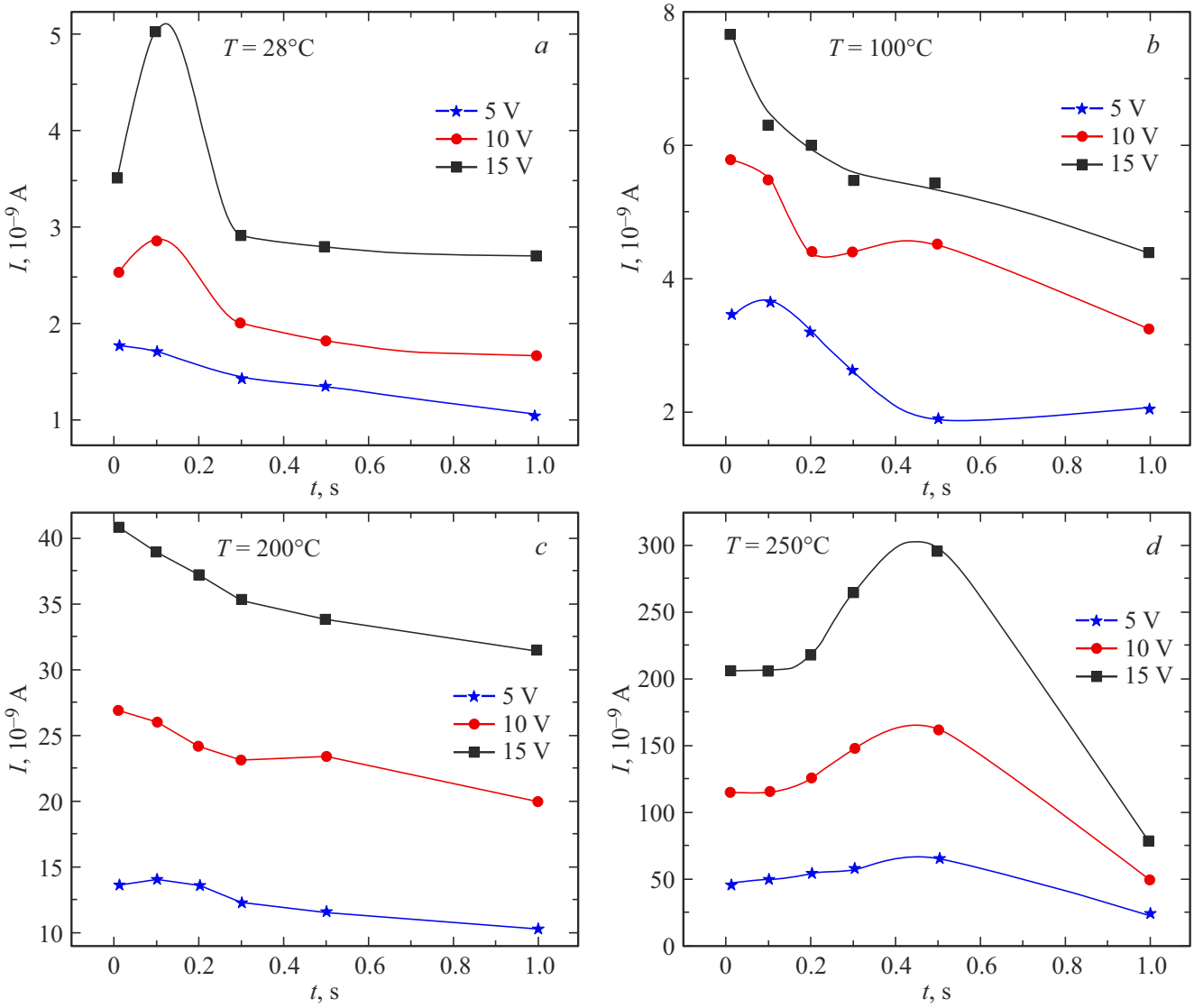

Figure 4. Leakage current vs. exposure time and electrical voltage at different temperatures.

the general case it is a function of temperature. The time τ is related to the trap energy E_t by the following relation [19]:

$$\tau = (\sigma \upsilon_T N)^{-1} \exp(E_t/kT), \qquad (2)$$

where σ — capture cross section, υ_T — average relative velocity of thermal motion of the charge relative to the trap, N — concentration of traps (defects). The capture cross section for charge carriers depends on the charge state of the trap and its value for attracting centers varies within the limits $\sim 10^{-18}$–10^{-16} m^2 [18]; the value N was determined from the slope of the direct capacitance-voltage (C-V) characteristic compiled in coordinates C^{-2}–V (Figure 7) and was equal to $\approx 2.8 \cdot 10^{20}$ m^{-3} (measurements $C(V)$ performed at room temperature); υ_T — (defined as $\upsilon_T = \sqrt{8kT/\pi m}$, m — electron mass) for low temperatures is $\approx 10^5$ m/s. N was calculated using the formula [19].

$$N = \frac{2}{g\varepsilon\varepsilon_0 S^2} \times \frac{\Delta u}{\Delta(1/C^2)}. \qquad (3)$$

Expression (3) when substituting the values of dielectric permittivity $\varepsilon \approx 100$ [20], dielectric constant ε_0 and contact area $S = 1.5 \cdot 10^{-6}$ m^2 gives the value $\approx 2.8 \cdot 10^{20}$ m^{-3}.

For $E_t = 0.51$ eV and $\sigma \approx 10^{-17}$ m^2 the estimate of τ using formula (2) leads to the value 0.49 s at room temperature, and at $T = 250$°C with the capture cross section $\sigma \approx 10^{-19}$ m^2 ($\sigma \propto 1/n\lambda$, $n \propto T$, n — electron concentration; λ — electron mean free path) τ for the same energy E_t numerically equal to ~ 0.26 s. Then we can assume that the rapidly decreasing sections $I(t)$ in Figure 4 ($T = 28$°C and $T = 100$°C) are due to the capture of current carriers at defect levels $E_t = 0.51$ eV over time ~ 0.5 s, and the observed current rise in $I(t)$

(Figure 4, $T = 250°C$) after time $t \geq 0.2$ s after voltage application — releasing captured carriers from the given level. Consider that curves $I(t)$ observed in Figure 6 are not direct oscillographic patterns, but are plotted on the basis of CVC data measured with different time delays.

In the case of Schottky emission, with electric field increasing the barrier W_b shall decrease, and in the insert of Figure 6 we see the opposite situation inherent to the Poole-Frenkel mechanism: as the electric field increases, electron emission occurs from more deep levels located in the band gap of the dielectric. The leakage current mechanisms listed above are not mutually exclusive; they operate in parallel, and one of them prevails depending on external conditions.

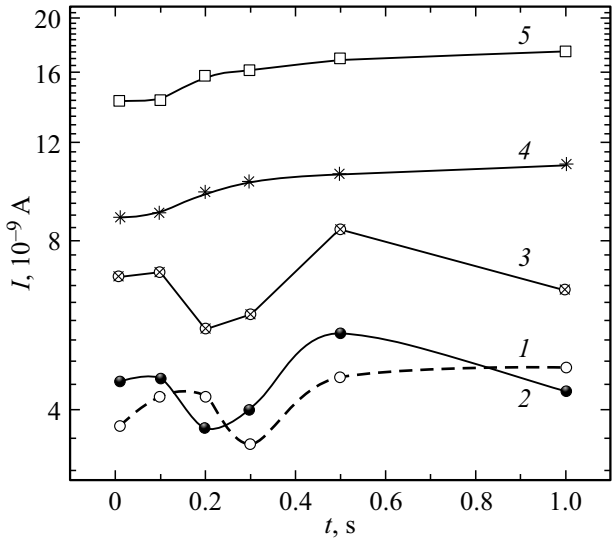

Figure 5. Current evolution after the voltage is reset to zero, curves *1*–*5* at 5, 6, 9, 11, 15 V, respectively.

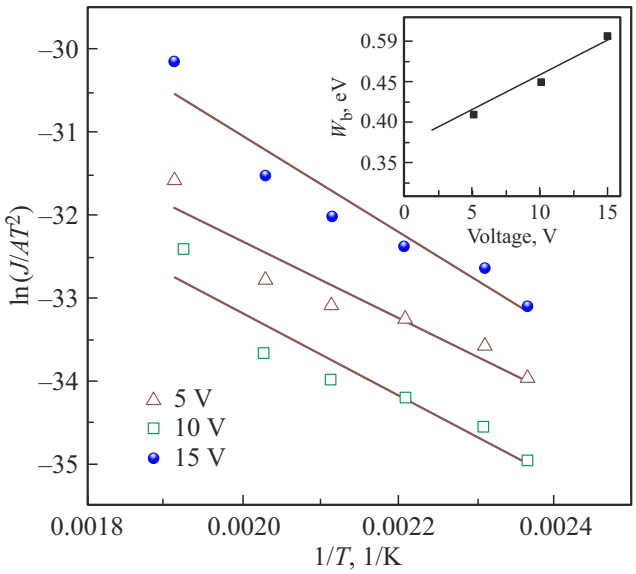

Figure 6. Linear approximation $\mathrm{Ln}(J/AT^2) - 1/T$ for the Schottky current from room temperature to 250°C at different external voltages. Insert shows the Schottky barrier extracted from the slope of the straight line $\mathrm{Ln}(J/AT^2) - 1/T$ as a function of voltage.

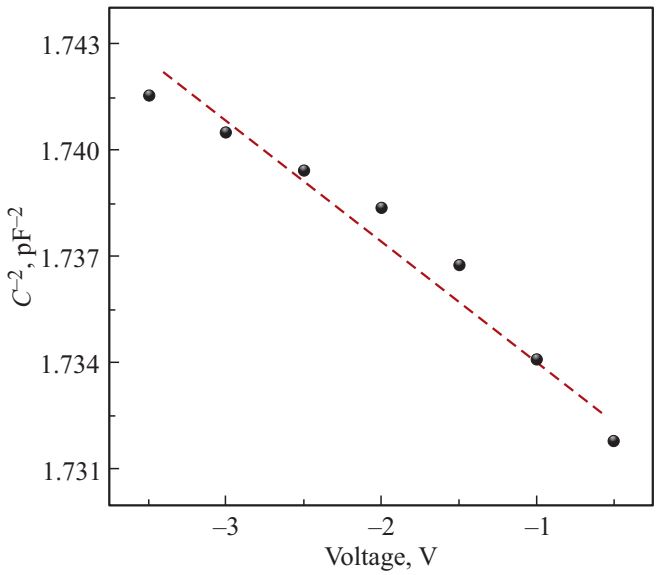

Figure 7. $C(V)$-characteristic of the sample in the region of negative displacements in coordinates $1/C^2 - V$.

4. Conclusion

Measuring CVC of thin films of BFTO dielectric according to the scheme: voltage generation–delay–measurement makes it possible to establish the dependence of the leakage current on the time of exposure to constant voltage and its magnitude. Analysis of this dependence revealed characteristic features at $t = 0.5$ s in the form of a tendency towards the occurrence of maximum $I(t)$ in the temperature range ~ 28–$200°C$. At temperature $T = 250°C$ the maximum in the time dependence stabilizes and begins to grow monotonically with applied voltage increasing. Thus, for this structure, we determined the characteristic time $t = 0.5$ s for the dependencies $I(t)$ due to the capture and release of carriers from defective levels.

Funding

This study was supported by a grant from the Russian Science Foundation, project No. 23-22-00421.

Conflict of interest

The authors declare that they have no conflict of interest.

References

[1] D.A. Abdullaev, R.A. Milovanov, R.L. Volkov, N.I. Borgardt, A.N. Lantsev, K.A. Vorotilov, A.S. Sigov. Ros. tekhnol. zhurn., **8**, *5*, 44 (2020). (in Russian).

[2] Alexander Cardona Rodríguez, Isabel C. Arango, Maria F. Gomez, Claribel Dominguez, Juan Trastoy, Christian Urban, Soumitra Sulekar, Juan C. Nino, Ivan K. Schuller, Maria E. Gomez, Juan Gabriel Ramírez. Solid State Commun. **288**, 38 (2019).
[3] J. Wang, J.B. Neaton, H. Zheng, V. Nagarajan, S.B. Ogale, B. Liu, D. Viehland, V. Vaithyanathan, D.G. Schlom, U.V. Waghmare, N.A. Spaldin, K.M. Rabe, M. Wuttig, R. Ramesh. Science **299**, 1719 (2003).
[4] W. Eerenstein, F.D. Morrison, J. Dho, M.G. Blamire, J.F. Scott, N.D. Mathur. Science **307**, 1203 (2005).
[5] J. Wang, A. Scholl, H. Zheng, S.B. Ogale, D. Viehland, D.G. Schlom, N.A. Spaldin, K.M. Rabe, M. Wuttig, L. Mohaddes, J. Neaton, U. Waghmare, T. Zhao, R. Ramesh. Science **307**, 5713 (2005).
[6] K.Y. Yun, M. Noda, M. Okuyama. Appl. Phys. Lett. **83**, 3981 (2003).
[7] Y.N. Venevtsev, G. Zhadanov, S. Solov'ev. Sov. Phys. Crystallogr. **4**, 538 (1960).
[8] G. Smolenskii, V. Isupov, A. Agranovskaya, N. Kranik. Sov. Phys. Solid State **2**, 2651 (1961).
[9] Zhen Zhao, Amr Abdelsamie, Rui Guo, Shu Shi3, Jianhui Zhao, Weinan Lin, Kaixuan Sun, Jingjuan Wang, Junling Wang, Xiaobing Yan, Jingsheng Chen. Nano Res. **15**, *3*, 2682 (2022).
[10] G.W. Pabst, L.W. Martin, Y. Chu, R. Ramesh. Appl. Phys. Lett. **90**, 072902 (2007).
[11] A.Q. Jiang, C. Wang, K.J. Jin, X.B. Liu, J.F. Scott, C.S. Hwang, T.A. Tang, H.B. Lu, G.Zh. Yang. Adv. Mater. **23**, 1277 (2011).
[12] F. Yang, F. Liu, F. Ji, Y. Lin, M. Tang. Mater. Adv. **1**, 2117 (2020).
[13] Y. Yang, H. Zhu, D. Chu, K. Liu, Y. Zhang, M. Pei, Sh. Feng, L. Jin, C. Wang, J. Liu, R. Li, Si Wang. J. Phys. D **53**, 115301 (2020).
[14] F. Orudzhev, Sh. Ramazanov, D. Sobola, A. Isaev, Ch. Wang, A. Magomedova, M. Kadiev K. Kaviyarasu. Nanomaterials **10**, 2183 (2020).
[15] S. Ramazanov, F. Orudzhev, G. Gajiev, V. Holcman, R. Matos, H. da Fonseca Filho, Ş. Tălu, D. Selimov. Appl. Surf. Sci. **647**, 158863 (2024).
[16] H. Yan, F. Inam, G. Viola, H. Ning, H. Zhang, Q. Jiang, T. Zeng, Zh. Gao, M.J. Reece. J. Adv. Dielectr. **1**, 107118 (2011).
[17] P.T. Oreshkin. Fizika poluporovodnikov i dielektrikov. Vyssh. shk., M., (1977). 448 s. (in Russian).
[18] S. Zi, Fizika poluprovodnikovykh priborov, Mir, M., (1984), T. 1. 456 s. (in Russian).
[19] L.P. Pavlov. Metody izmereniya parametrov poluprovodnikovykh materialov. Vyssh. shk., M., (1987). 239 s. (in Russian).
[20] J. Kolte, P.H. Salame, A.S. Daryapurkar, P. Gopalan. AIP Advances **5**, 097164 (2015).

Translated by I.Mazurov